energies

MDPI

Article

Relationships between Dynamic Elastic Moduli in Shale Reservoirs

Sheyore John Omovie [1] and John P. Castagna [2,*]

[1] Petrophysics Department, Formerly with OXY, Houston, TX 77046, USA; john.omovie@gmail.com
[2] Earth and Atmospheric Sciences, University of Houston, 4800 Calhoun Rd, Houston, TX 77004, USA
* Correspondence: jpcastagna@uh.edu

Received: 18 October 2020; Accepted: 10 November 2020; Published: 17 November 2020

Abstract: Sonic log compressional and shear-wave velocities combined with logged bulk density can be used to calculate dynamic elastic moduli in organic shale reservoirs. We use linear multivariate regression to investigate modulus prediction when shear-wave velocities are not available in seven unconventional shale reservoirs. Using only P-wave modulus derived from logged compressional-wave velocity and density as a predictor of dynamic shear modulus in a single bivariate regression equation for all seven shale reservoirs results in prediction standard error of less than 1 GPa. By incorporating compositional variables in addition to P-wave modulus in the regression, the prediction standard error is reduced to less than 0.8 GPa with a single equation for all formations. Relationships between formation bulk and shear moduli are less well defined. Regressing against formation composition only, we find the two most important variables in predicting average formation moduli to be fractional volume of organic matter and volume of clay in that order. While average formation bulk modulus is found to be linearly related to volume fraction of total organic carbon, shear modulus is better predicted using the square of the volume fraction of total organic carbon. Both Young's modulus and Poisson's ratio decrease with increasing TOC while increasing clay volume decreases Young's modulus and increases Poisson's ratio.

Keywords: elastic moduli; shale reservoirs; sonic velocities; Poisson's ratio; Young's modulus

1. Introduction

Sonic velocity and density logs provide direct in situ measurement of formation dynamic moduli and derived quantities. Given compressional-wave velocity, density, and measured or estimated shear-wave velocity, dynamic bulk, P-wave, Young's and shear moduli and Poisson's ratio can be directly calculated [1]. With sufficient calibration, these dynamic moduli can potentially be used to estimate static moduli and, especially if anisotropy can also be quantified, they may be useful for hydraulic fracturing design in shale reservoirs [2].

Dynamic bulk (k) and shear (μ) moduli are determined directly from acoustic velocities and density by

$$\mu = \rho V_s^2, \tag{1}$$

and

$$k = \rho V_p^2 - 4\mu/3, \tag{2}$$

while the P-wave modulus (M) is simply

$$M = \rho V_p^2 = k + 4\mu/3, \tag{3}$$

where V_p is compressional-wave velocity, V_s is shear-wave velocity, and ρ is rock bulk density. Of more direct interest in engineering applications are Poisson's ratio, ν, and Young's modulus, E, given by

$$\nu = (k/\mu - 2/3)/(2k/\mu + 2/3) = (V_p/V_s{}^2 - 2)/(2V_p/V_s{}^2 - 2), \quad (4)$$

and

$$E = 2\mu\,(1 + \nu). \quad (5)$$

The ratio k/μ is related to the V_p/V_s ratio by

$$k/\mu = (V_p/V_s)^2 - 4/3. \quad (6)$$

There is a one-to-one relationship between Poisson's ratio, the velocity ratio, and the bulk-to-shear moduli ratio. We can expect these ratios to be dependent on rock and fluid properties, such as porosity, mineralogy, total solid organic carbon (TOC), fluid compressibility, and effective pressure as well as factors less readily quantifiable from logs such as texture, pore, and inclusion shape, organic matter maturity, and degree of lithification/cementation.

As the velocities are measured at sonic frequencies with acoustic signals exhibiting small strain amplitudes, dynamic moduli are generally not equal to static (zero-frequency) elastic moduli [3] but may provide useful indication of Young's modulus and Poisson's ratio variations along a borehole [4] as well as estimation of formation brittleness [5]. Empirical relations can be used to convert dynamic to static moduli [6] but care must be taken to consider anisotropic and pressure effects when doing so [7]. Deviations of these moduli from expectations, as evidenced on sonic compressional-wave and shear-wave sonic logs, may provide useful lithologic insights in formation evaluation [8–10].

There are numerous other studies relating velocities and/or elastic moduli to rock properties in shale reservoirs (for example [11–25]). Factors affecting velocities and moduli include, but are not limited to, mineral composition, porosity, solid organic volume, pore fluid content, properties and saturation, effective pressure, degree of lithification/cementation and organic maturity, structural arrangement and distribution of constituents, and pore and grain shape spectra. As a practical matter, there are generally too many unknowns to reliably predict velocities directly from rock properties and environmental conditions without local calibration. However, in conventional reservoirs and inorganic shales, it is well established that many rock properties and environmental factors, though directly having a strong effect on velocities and moduli, may have a reduced effect on relationships between velocities or moduli (see for example [8,26]). This enables shear-wave velocity prediction from given compressional-wave velocity and compositional volumetrics with good precision and accuracy without explicit consideration of all the factors affecting velocities listed above [27]. In this paper, we have selected seven different shale reservoirs to empirically study, and generalize across a variety of formations, the factors controlling velocity and moduli relationships and to determine the most significant factors that cause variation in these relationships within and between formations. The objective is to arrive at more universal relationships that can be applied with good accuracy and precision without calibration by locality, formation, or degree of maturity.

2. Materials and Methods

As unconventional shale reservoirs are generally highly anisotropic [28,29] we here restrict our analysis to bedding normal velocities measured by sonic logs in vertical wells in formations with nearly horizontal dip. For wells or formations with different orientations, correction for anisotropy may be necessary.

Our objective is to develop an interpretive framework based on the relationships between dynamic moduli using empirical observation and regression analysis. We utilized a database consisting of full well-logging suites in single vertical pilot wells in seven different shale reservoirs including the Spraberry, Wolfcamp, Avalon, Woodford, Eagle Ford, Cline, and Bakken formations. The well logs

included reliable compressional and shear-wave sonic logs and core-calibrated volumetric well log analyses (for further description of the quantitative well log analysis performed, see [9]). These reservoirs have a wide range of rock and fluid properties as determined by volumetric well log analysis (summarized in Figure 1, Tables 1 and 2 for our dataset) yet similar relationships between compressional-wave velocity and shear-wave velocity (see Figure 2 and Table 3). The spread of the compositional variation by formation is indicated by the standard deviations around the mean compositions (Table 1). Comparisons of well log volumetric analyses to core measurements for these formations are provided in prior papers [9] and [27] and in Figure 3 for an interval in the Wolfcamp shale. Table 4 shows that the V_p-V_s relationship (see Figure 2) derived here from logs in organic shale reservoirs is close to trends from laboratory measurements for both dry organic and dry inorganic shales with low total organic content (TOC) reported in [9]. Our dataset only samples these formations at one locality for each formation so is not meant to be representative of these formations over a wide geographic area. For our dataset, the Spraberry, Wolfcamp, Woodford, and Cline formations have similar composition and pore fluid (volatile oil). The Woodford is somewhat different in that it has no carbonate content and the lowest average porosity of all the formations. The dominant constituent of the Eagle Ford is calcite, and it is the only log in our dataset over a producing gas reservoir. The Bakken has the highest TOC and produces black oil. The Avalon has the highest average quartz content in the dataset.

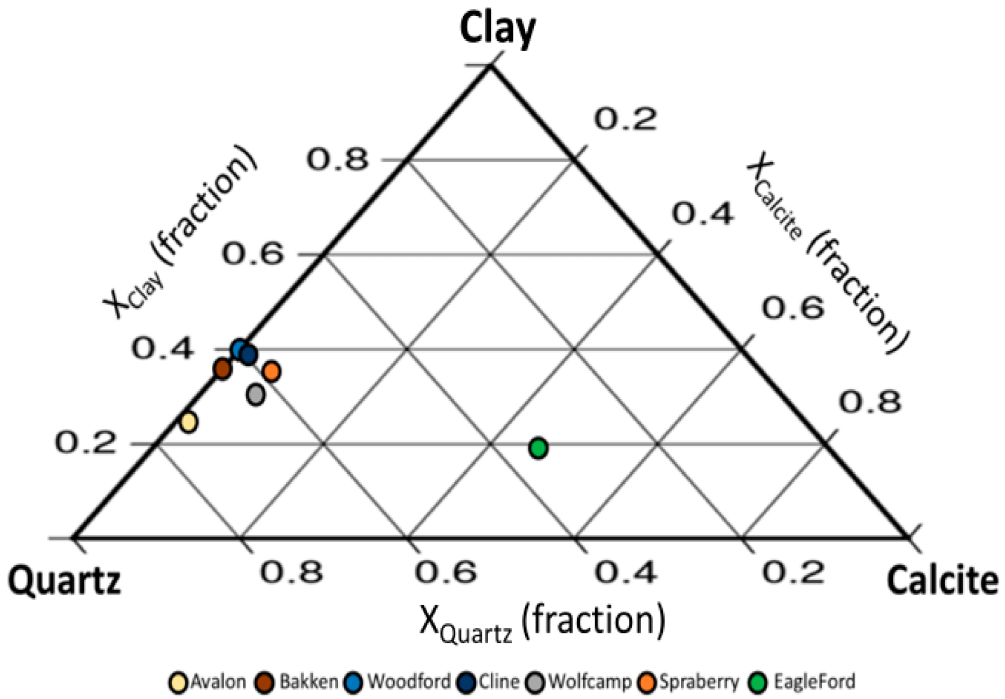

Figure 1. Ternary volume fraction composition diagram for average formation properties in our dataset for shale reservoirs in the quartz–clay–calcite system with the volume fractions normalized to sum to unity. Other constituents are neglected on this diagram. The Eagle Ford is compositionally a dirty limestone. The Avalon is abnormally quartz rich. The Woodford has zero calculated calcite. The Bakken has no computed calcite but has significant dolomite content and high TOC.

Table 1. Average rock properties from well logs for shale reservoirs studied here. Each formation is represented by only single wells, so these values are not meant to be representative of the entire geographic extent of the formations. High water saturations (greater than 70%) and low TOC volume fractions (less than 1%) are excluded. Reported quantities are mean values for included depths. Depth is mean depth for included datapoints in each formation. Density is mean logged density. V_p and V_s are mean sonic compressional and shear-wave velocities. R_o is percent vitrinite reflectance determined from cuttings and S_w is mean decimal water saturation from log analysis. The X_i are mineral solid volume fractions from volumetric log analysis such that $\sum X_i = 1$ for organic matter (X_{TOC}) pyrite (X_{Pyrite}), calcite ($X_{Calcite}$), dolomite ($X_{Dolomite}$), clay (X_{Clay}), and quartz plus feldspars (X_{Quartz}). TOC is weight percent of total solid organic carbon. X_{TOC} is the volume fraction of solid organic carbon derived from TOC using the Vernik relation [30] which is Equation (6) in [27]. The depth range is the top and base of the logged interval. ϕ_{Total} is total porosity using measured log density and grain density from solid volume fractions. Standard deviations for volumetric well log calculations of shale reservoirs studied here. Standard deviations corresponding to mean values given above for decimal volume fractions of solid organic matter (X_{TOC}), pyrite (X_{Pyrite}), calcite ($X_{Calcite}$), dolomite ($X_{Dolomite}$), clay (X_{Clay}) and quartz plus feldspars (X_{Quartz}), total porosity (ϕ_{Total}), and water saturation (S_w).

Formation	Depth	Density	V_p	V_s	V_p/V_s	μ	κ	TOC	Depth Range
	m	gm/cc	km/s	km/s	ratio	GPa	GPa	wt. %	m
Spraberry	2007	2.54	3.74	2.17	1.72	12.04	19.68	2.88	1962-2046
Wolfcamp	2350	2.54	3.73	2.16	1.73	11.84	19.74	3.71	2326-2374
Avalon	2380	2.46	3.77	2.34	1.61	13.60	17.24	7.61	2337-2423
Woodford	3193	2.52	3.51	2.11	1.66	11.25	16.02	5.58	3188-3200
Eagle Ford	3886	2.55	4.06	2.39	1.70	14.60	22.67	2.88	3838-3928
Cline	2807	2.52	3.70	2.24	1.66	12.64	17.82	6.07	2772-2831
Bakken	3381	2.28	3.05	1.84	1.66	7.75	11.01	14.44	3371-3391
Formation	**X_{TOC} decimal**	**X_{Pyrite} decimal**	**$X_{Calcite}$ decimal**	**$X_{Dolomite}$ decimal**	**X_{Clay} decimal**	**X_{Quartz} decimal**	**ϕ_{Total} decimal**	**S_W decimal**	**R_0 percent**
Spraberry	0.05	0.03	0.09	0.00	0.33	0.49	0.10	0.54	0.80
Wolfcamp	0.07	0.03	0.11	0.00	0.27	0.51	0.08	0.44	0.80
Avalon	0.14	0.03	0.02	0.02	0.20	0.60	0.07	0.30	0.94
Woodford	0.11	0.03	0.00	0.00	0.35	0.53	0.04	0.47	0.98
Eagle Ford	0.06	0.01	0.60	0.00	0.18	0.15	0.08	0.49	1.80
Cline	0.12	0.03	0.03	0.01	0.32	0.48	0.06	0.55	0.98
Bakken	0.26	0.03	0.00	0.12	0.21	0.38	0.07	0.24	1.30
Formation	**X_{TOC} decimal**	**X_{Pyrite} decimal**	**$X_{Calcite}$ decimal**	**$X_{Dolomite}$ decimal**	**X_{Clay} decimal**	**X_{Quartz} decimal**	**ϕ_{Total} decimal**	**S_W decimal**	
Spraberry	0.010	0.008	0.085	0.000	0.071	0.087	0.013	0.077	
Wolfcamp	0.012	0.006	0.126	0.000	0.060	0.077	0.016	0.094	
Avalon	0.032	0.007	0.070	0.048	0.065	0.073	0.017	0.083	
Woodford	0.016	0.009	0.000	0.000	0.077	0.083	0.008	0.148	
Eagle Ford	0.016	0.009	0.092	0.000	0.061	0.064	0.014	0.098	
Cline	0.033	0.007	0.066	0.045	0.077	0.076	0.008	0.177	
Bakken	0.033	0.009	0.000	0.091	0.053	0.069	0.024	0.073	

Table 2. Average fluid properties for the shale reservoirs studied here. Moduli are based on the Batzle and Wang [31] equations ((8) to (10)) for gas and ((20) to (24)) for oil and adjusted for composition and in situ pressure and temperature. By volatile oil we mean gas/oil ratios above 1000 standard cubic feet per barrel and an API gravity of 40° or greater.

Formation	Hydrocarbon Type	Hydrocarbon Bulk Modulus	Hydrocarbon Density	Brine Bulk Modulus	Brine Density	Mean Temperature	Pore Pressure
		GPa	gm/cc	GPa	gm/cc	°F	MPa
Spraberry	Volatile Oil	0.375	0.675	2.750	1.050	113	21
Wolfcamp	Volatile Oil	0.434	0.677	2.730	1.050	121	28
Avalon	Volatile Oil	0.366	0.670	2.750	1.050	121	30
Woodford	Volatile Oil	0.430	0.675	2.750	1.050	155	36
Eagle Ford	Gas	0.130	0.250	2.800	1.050	199	53
Cline	Volatile Oil	0.430	0.675	2.750	1.050	130	35
Bakken	Oil	0.750	0.800	3.350	1.120	176	46

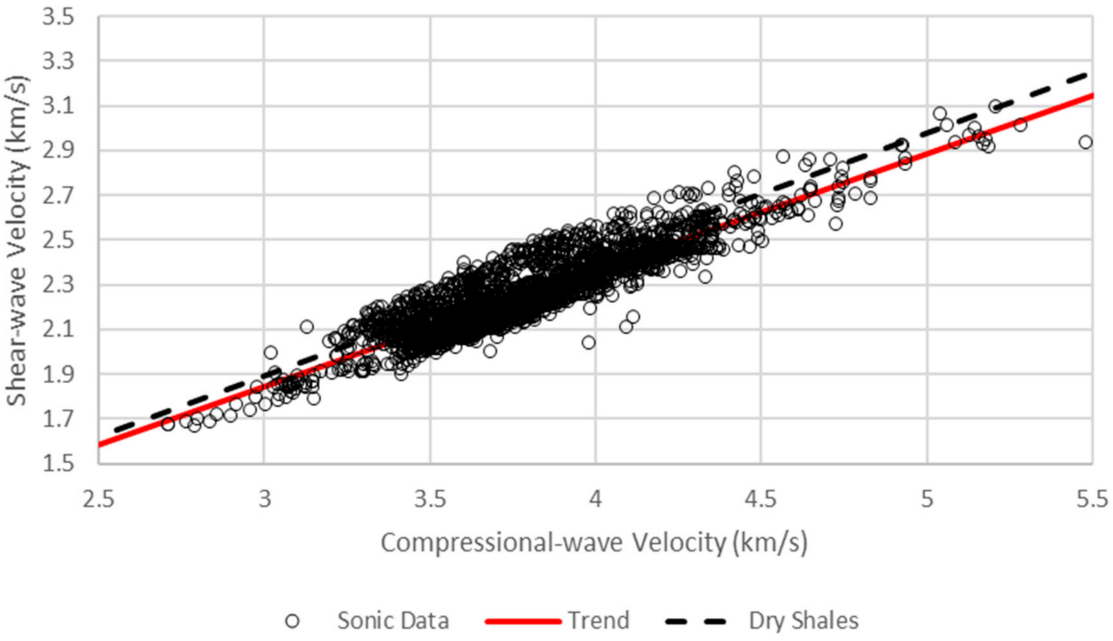

Figure 2. Shear-wave velocity (V_s)versus compressional-wave velocity (V_p) cross plot for sonic log measurements in seven organic-rich shale reservoirs containing fluid hydrocarbons with water saturations below 70%. The red solid line is the least mean-squared error (LMSE) fit to the data (V_s = 0.520 V_p + 0.287 km/s). The correlation coefficient is 0.9 and the mean absolute error is 2.9%. The regression is highly statistically significant with an F-test (ratio of explained to unexplained variance) of over 8000 and *sig* F (the probability that the calculated correlation is fortuitous) of zero. The dashed black line is the LMSE trend for dry organic shale laboratory measurements reported in [9]. The point cloud contains multiple closely spaced nearly parallel trends that are slightly offset from the general trend in different formations (see Table 3).

Table 3. Shear-wave velocity (V_s) versus compressional-wave velocity (V_p) relationships by formation. Velocities are in km/s. R is the correlation coefficient and std error is the standard deviation of the prediction residual. The F-test was greater than 100 and the sig F statistic was virtually zero in all cases. The trends are similar excepting the Woodford shale which can be explained as a binary sequence of layers alternating between siliceous and organic mudrock. Velocities are in units of km/s.

Formation	Regression Equation	R	std Error (km/s)
Spraberry	$V_s = 0.497\ V_p + 0.313$	0.91	0.042
Wolfcamp	$V_s = 0.518\ V_p + 0.222$	0.92	0.044
Avalon	$V_s = 0.514\ V_p + 0.402$	0.94	0.076
EagleFord	$V_s = 0.489\ V_p + 0.403$	0.94	0.042
Woodford	$V_s = 0.898\ V_p - 1.04$	0.98	0.024
Cline	$V_s = 0.453\ V_p + 0.563$	0.90	0.044
Bakken	$V_s = 0.497\ V_p + 0.313$	0.86	0.040

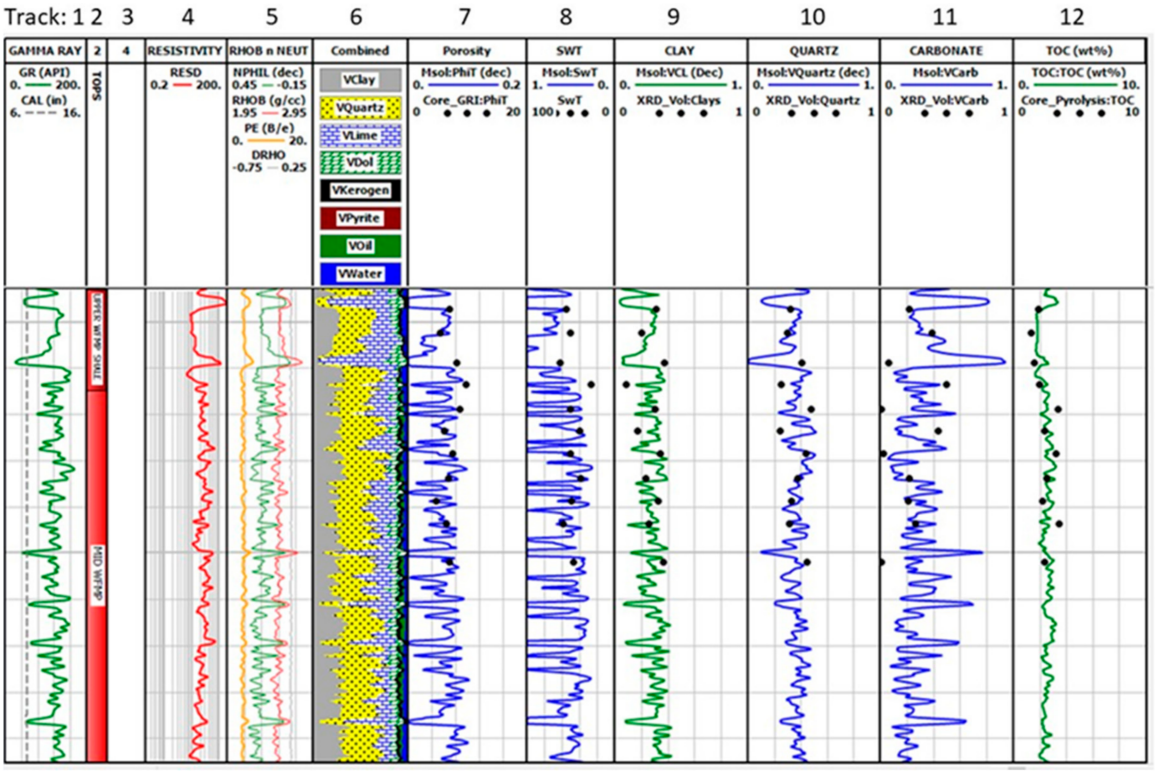

Figure 3. Well log volumetric analysis in the Wolfcamp Formation compared to core X-ray diffraction, fluid volume, and pyrolysis results showing good average agreement in prediction of porosity, water saturation, clay volume, and TOC weight%. The log analysis procedure is described in (9). The carbonate volume fraction log versus core comparison is misleading due to differences in vertical resolution between the core and well logs, however, the directions of the changes are consistent between logs and core. The vertical depth interval displayed is 200 feet (61 m). Track numbers are from left to right. Track 1: Gamma-ray (GR—solid green curve)) in API units and Caliper (CAL—dashed gray curve) in inches. Track 2: Formation name differentiating Upper Wolfcamp Shale (Upper WFMP Shale) and Middle Wolfcamp Shale (Mid WFMP). Track 3: Blank track. Track 4: Deep resistivity (RILD) in ohm-m. Track 5: Neutron porosity in decimal limestone units (NPHIL—green curve), formation bulk density in gm/cc (RHOB—red curve), and photoelectric effect on barns/e (PE—orange curve). Track 6: Volumetric well-log analysis in fractional decimal units. Volume clay (VClay) in gray, volume of quartz (VQuartz) is dotted yellow, volume of calcite (VLime) is blue bricked, volume of dolomite (VDol) is green bricked,

volume of kerogen (VKerogen) is black, volume pyrite (VPyrite) is maroon, volume of oil (Voil) is green, and volume of water (porosity) is blue. Track 7: Calculated decimal total porosity (Msol:PhiT, blue curve) in decimal fraction and GRI core total porosity (Core_GRI: PhiT, black dots) in porosity units (PU). Track 8: Calculated decimal volume fraction of water saturation from logs (Msol:SWT, blue curve) and percentage water volume extracted from cores (SWT, black dots). Track 9: Calculated decimal volume fraction of clay (Msol:VCL, green curve) from logs and core X-ray diffraction volume of clay (XRD_Vol:Clays, black dots). Track 10: Calculated decimal volume fraction of quartz (Msol:Vquartz), blue curve and core X-ray diffraction decimal volume of quartz (XRD_VQuartz). Track 11: Calculated decimal sum of calcite and dolomite fractions (Msol:VCarb, blue curve) and core X-ray diffraction decimal volume of carbonate (XRD_Vcarb, black dots). Track 12: Calculated weight percent total organic carbon from logs (TOC, green curve) and core pyrolysis weight percent (Core_pyrolysis:TOC, black dots.).

Table 4. Shear-wave velocity (V_s) versus compressional-wave velocity (V_p) relationships. From (**a**) measured velocity logs in organic shale reservoirs, (**b**) bedding normal laboratory measurements in dry organic shales, and (**c**) bedding normal laboratory measurements on dry inorganic shales from the offshore Gulf of Mexico. The laboratory measurements are from [9]. Velocities are in units of km/s.

Description	Regression Equation
(a) in situ shale reservoirs from logs	$V_s = 0.520\ V_p + 0.287$
(b) dry organic shales	$V_s = 0.544\ V_p + 0.263$
(c) dry inorganic marine shales	$V_s = 0.527\ V_p + 0.282$

We studied how variable composition impacts relationships between dynamic moduli by performing multivariate linear regression analysis and related statistical tests using the Microsoft™ EXCEL software product. The equations for statistical quantities used in this paper are provided in Appendix A. Regressions were performed on various subsets including all wells combined, specific formations, and averages for each formation. To isolate controlling variables strictly within the shale reservoir rock while considering uncertainty in water saturation calculations, we excluded from our analysis datapoints with water saturations greater than 70% as well as low TOC intervals with weight percent of total organic content less than 1%. We also excluded datapoints within the logging tool spatial resolution of boundaries with non-reservoir layers. The resulting data spreadsheet we used to perform regressions is included in supplementary materials Table S1.

3. Results

Given that density and compressional-wave velocity are often highly correlated [32] the well-defined $V_s - V_p$ relationships in Figure 2 and Table 3 suggest that, as V_p is a good predictor of V_s when shear sonic logs are not available [27], dynamic elastic moduli should also be correlated. This correlation can be seen in Figures 4 and 5 and Table 5, where individual formations show similar but distinct relationships between dynamic bulk and shear moduli. In comparison to the velocity trends, which are for the most part similar and well defined, the dynamic elastic moduli trends exhibit more variation in slope and intercept, lower correlation coefficients, and greater prediction error. This may be due to the less well-defined relationship between velocities and densities that may introduce variability into the modulus trends.

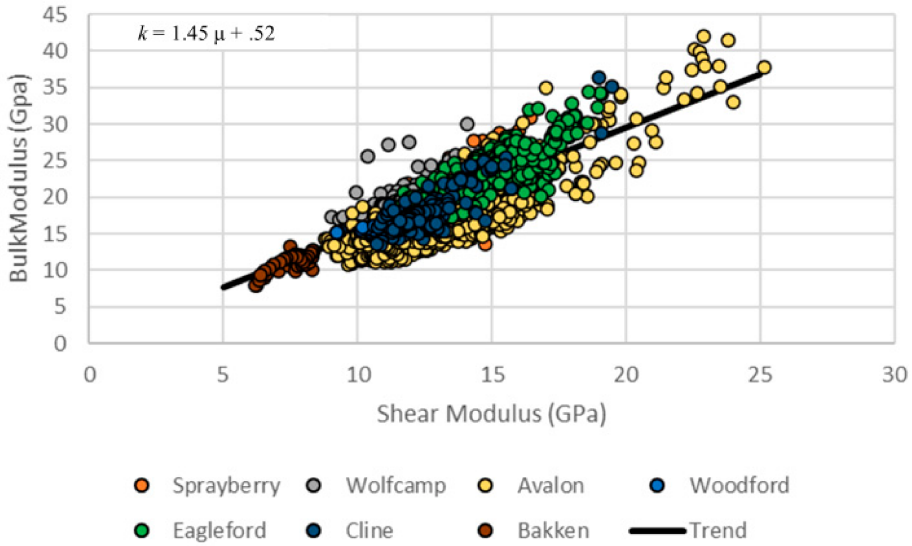

Figure 4. Overall bulk modulus (k) versus shear modulus (μ) trend for well log measurements from all reservoirs studied. V_p, V_s, and ρ logs were used to calculate dynamic moduli using Equations (1)–(3). As there are over 2000 closely spaced datapoints following the predominant trend, the points primarily overlay. The difference in behavior for different formations is better seen in Figure 5. The least-mean-square regression fit for all formations combined is k = 1.45 u + 0.52 for moduli in GPa. The correlation coefficient is 0.78, the F-test is over 3000, sig F is zero, and the standard error is 2.79 GPa. Improved standard error requires local calibration or correction for lithologic and pore fluid effects.

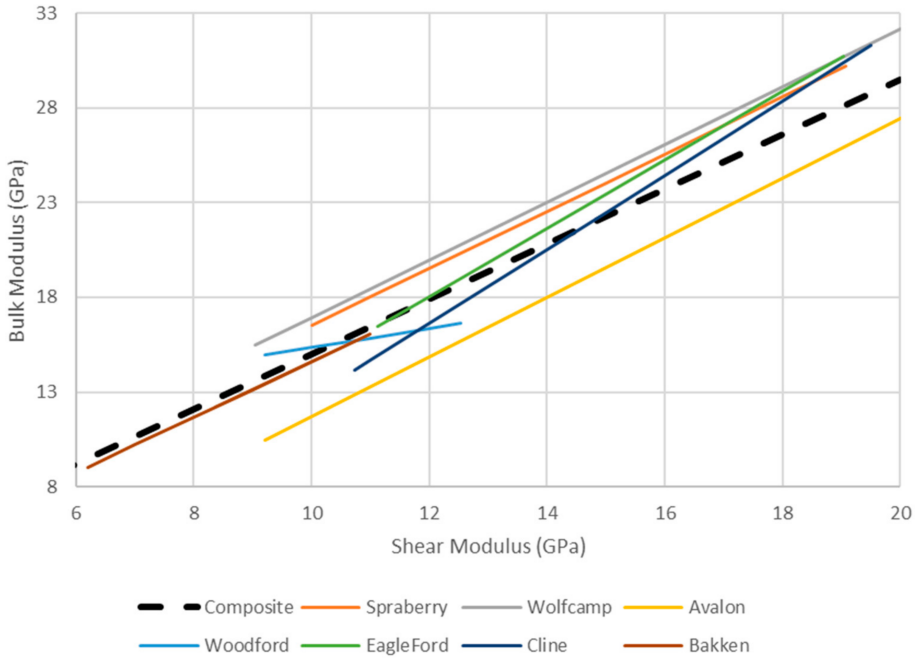

Figure 5. Formation specific dynamic bulk modulus (k) versus shear modulus (μ) trends for the seven shale reservoirs compared to the composite overall trend (dashed line) from Figure 4. The different formations have specific k versus μ trends displayed here (and given in Table 5) related to differing lithological factors discussed below. All trends are statistically significant. The Woodford trend has an anomalous slope due to interbedding between organic shales (which have smaller moduli) and siliceous low TOC layers (which have greater moduli and a smaller k/μ ratio). The Avalon trend has an anomalously low intercept and k/μ ratio consistent with its anomalously high quartz content.

Table 5. Bulk modulus (k) versus shear modulus (μ) relationships by formation'. Moduli are given in GPa. R is the correlation coefficient and std error is the standard deviation of the prediction residual. The F-test was greater than 100 and the sig F statistic was virtually zero in all cases. The trends are similar excepting the Woodford shale. The mean absolute error for all datapoints using these individual relationships is 1.7%. The anomalous Woodford Shale relationship can be explained as being due to interbedding of siliceous and non-siliceous thin layers. Moduli are in GPa.

Formation	Regression Equation	R	std Error (km/s)
Spraberry	$k = 1.51\mu + 1.42$	0.78	1.49
Wolfcamp	$k = 1.52\mu + 1.72$	0.80	1.49
Avalon	$k = 1.58\mu - 4.10$	0.86	2.72
Woodford	$k = 0.50\mu + 10.3$	0.67	0.58
Eagle Ford	$k = 1.81\ \mu - 3.63$	0.87	1.69
Cline	$k = 1.95\mu - 6.79$	0.84	1.78
Bakken	$k = 1.46\mu - 0.03$	0.77	0.75

To predict shear modulus when only compressional wave-velocity and density are logged, bivariate regression for shear modulus (see Figure 6) gives

$$\mu = 0.306\ \rho V_p^2 + 1.76, \quad (7)$$

where velocity is given in km/s, density is in gm/cc, shear modulus is in GPa, and ρV_p^2 is the P-wave modulus M. The tighter fit and higher correlation than that obtained for the bulk modulus relation can be attributed in part to the greater range of P-wave modulus values.

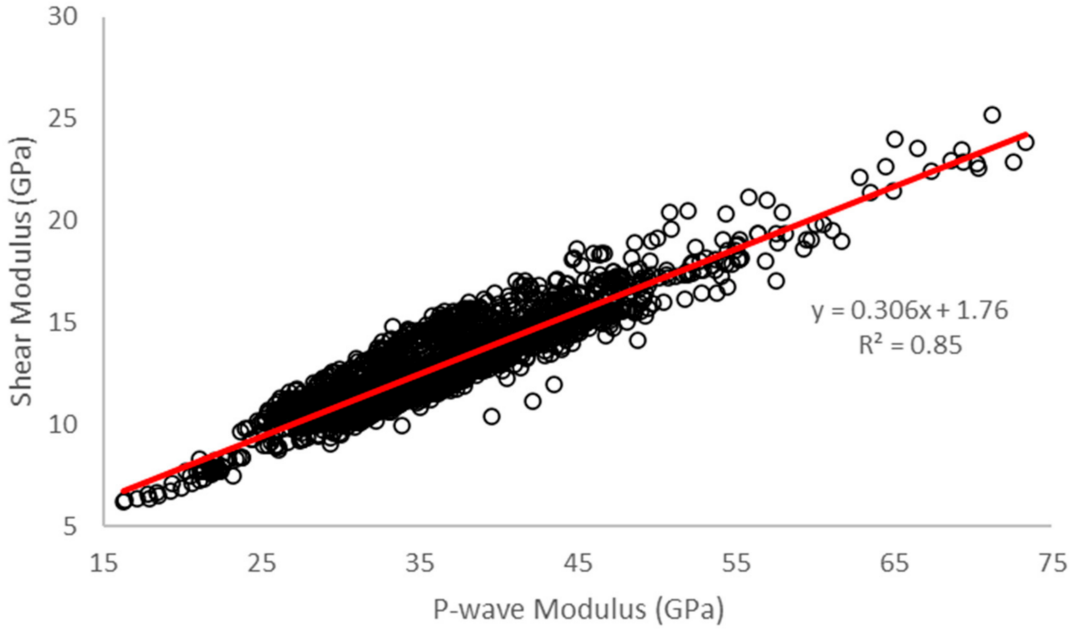

Figure 6. Dynamic shear modulus versus dynamic P-wave modulus for all formations combined from sonic and density log measurements. The least-mean-square error trendline is $\mu = 0.306\ M + 1.76$ for units in GPa. The correlation coefficient is 0.92 and the std error of the prediction is 0.92 GPa. The F-statistic is over 11,000 and *sig* F is 0. This trend provides a useful estimation of dynamic shear modulus given only V_p and ρ but can be refined with correction for composition (see below).

A dominant factor determining the k-μ or M-μ relationships (and perhaps more importantly deviations from a single relationship for a formation in a specific locality) is the mineralogical composition. The relationships in Table 5 are dependent to a large extent on the average composition of the formation at the well location.

The compositional dependence can be summarized statistically for the entire dataset via linear multiple regression. We regressed moduli against all lithologic parameters including mineral composition, TOC (total organic carbon), porosity, and fluid modulus, saturations, and bulk volumes. Of note, in our dataset we found no statistically significant relationship between observed bulk modulus or P-wave modulus and fluid properties. This can be explained by the exclusion of water saturations above 70%, as within reservoir rock containing hydrocarbons the variation of moduli with water saturation is small compared to the difference in moduli between fully-water saturated and partially water-saturated shales [9].

A small improvement over Equation (7) in prediction of shear-modulus can be achieved by accounting for the compositional dependence. Multiple regression in units of GPa and decimal volume fraction yields

$$\mu = 0.34\,M + 8.77\,X_{TOC} - 2.95\,X_{CLAY} - 0.97\,X_{CARB} + 0.56, \quad (8)$$

where, X_{TOC} is the volume fraction of organic matter converted from weight percent TOC using the Vernik [30] method, X_{CLAY} is the volume fraction of clay minerals from log analysis as described in [9], and X_{CARB} is also derived from volumetric log analysis and taken as the sum of carbonate volume fractions (calcite and dolomite) plus the volume fraction of pyrite which was too small in number or range to stand alone as a regression variable and therefore lumped with carbonates due to its high density. The correlation coefficient for the regression is 0.95 and the standard error of the predicted shear modulus is 0.77. The regression is highly significant with an F of 4424 and a sig F of 0.

Equation (8) indicates that for a given P-wave modulus, increasing TOC increases the shear modulus (corresponding to a reduced M/μ and thus reduced V_p/V_s ratio) and the shear modulus decreases with increasing clay or carbonate content at a given P-wave modulus (corresponding to in increased M/μ and V_p/V_s ratio). As discussed in [9], the effects of fluid hydrocarbons and TOC are intimately intertwined and difficult to separate. To first order, those effects are apparently combined in the TOC effect evident in Equation (8).

Predicting moduli from volumetric analysis alone (without dynamic P-wave modulus as input) as a function of depth is more challenging as the P-wave modulus implicitly contains and accounts for local variation in factors such as porosity, pore shape, effective pressure, and degree of lithification. The best statistically significant correlations we could find were on the order of 0.8 for shear modulus and 0.85 for bulk modulus. We do not report those relationships here as they can be easily misapplied as they would be highly locality and formation dependent. We did, however, wish to investigate the compositional dependence of average formation properties. Perhaps surprisingly, when weighting all shale reservoir formations equally, we found excellent (and the most statistically significant) results for average formation properties using only TOC and clay volume fractions. For bulk modulus, the regression fit for average formation properties and weighting all formations equally in units of GPa and decimal volume fraction is

$$k = 28.2 - 52.0\,X_{TOC} - 17.0\,X_{CLAY.} \quad (9)$$

The correlation coefficient is a remarkable 0.99 with an F statistic (ratio of explained to unexplained variance) of 68.7, and the significance of F (probability that the correlation is spurious by random chance) being less than 0.001. The standard error in the predicted average bulk modulus is 0.75 GPa. Increasing organic content or volume of clay both decrease the bulk modulus with the dependence on TOC being about 3 times stronger. Neither porosity, carbonate content, nor fluid properties improved the regression, which is surprising given that these factors have a clear effect on compressibility. We hypothesize that this is due to the non-independence of variables such that the effects of mineral composition, porosity, and fluid properties are intertwined with average volume fractions of TOC and clay; these two compositional variables are consequently sufficient to establish a correlation between average observations and predictions that would be difficult to improve upon. The insensitivity to fluids is not contrary to the findings in [9] which noted the difference in bulk modulus between

fully-brine saturated shales and reservoir shales with appreciable fluid hydrocarbons; the difference being that in the data presented here we have excluded all water saturations above 70%. The lack of dependence on carbonate content may be in part fortuitous, as in our dataset the single formation with anomalously large volume fraction of carbonate is also the only formation that produces gas, and these factors may cancel out. However, we would not expect such cancellation to occur for average formation shear modulus (which should be insensitive to pore fluid modulus) where, the same compositional variables are dominant (in units of GPa and decimal volume fraction)

$$\mu = 17.2 - 91.1\ X^2_{TOC} - 13.8\ X_{CLAY.} \quad (10)$$

The regression yields a dependence of shear modulus with X_{TOC} that is no longer linear but rather varies with the square of TOC volume fraction. The regression prediction for average formation properties has a correlation coefficient of 0.93 with an F of 12 and a significance of F of 0.02. The standard error is 1 GPa. The correlation is not quite as good as in predicting bulk modulus from these same variables and there is a 2% probability that the correlation can be caused by random chance. Nevertheless, this is an acceptable result in relating shear modulus to compositional variables with the error being tolerable for many applications (see for example [30] and [33]) and Equations (9) and (10) are best used as an indication of the systematics of variation of moduli with composition, rather than for prediction of absolute moduli.

The cross-plot of measured versus predicted average formation moduli (Figure 7) using Equations (9) and (10) shows some slight bias in some of the formations; suggesting that local recalibration is likely to be helpful, especially for different localities or formations. Given the other factors mentioned previously affecting moduli that are not accounted for in Equations (9) and (10) it is highly unlikely that these relations will hold far beyond the points of calibration or with very different rock properties or environmental conditions. We must emphasize that Equations (9) and (10) are intended to show relative changes in modulus that might be expected with a given change in composition rather than for the purpose of predicting moduli in absolute terms without local calibration. These trends are not expected to be universal; rather Equations (7) and (8) using the P-wave modulus should be used for predictive purposes.

Given that compressional-wave velocity is an excellent predictor of shear-wave velocity one might find it surprising that using the bulk modulus to predict shear modulus does not improve prediction of average reservoir properties. This is explained by the fact that, being so well related to volumes of organic carbon and clay via Equation (9), negligible additional information is provided by explicitly including the average bulk modulus. Consequently, including average bulk modulus as a regression variable reduces the statistical significance of the prediction of average shear modulus. As average bulk modulus is linear with X_{TOC} and average shear modulus is non-linear, we expect the ratio of average bulk and shear moduli (and the derived Poisson's ratio) to also vary non-linearly with total organic content.

The other dynamic elastic moduli of interest (assuming first order isotropy) can be computed directly from bulk and shear moduli using

$$E = 9k\mu/(3k + \mu), \quad (11)$$

for Young's modulus (E), and

$$\nu = E/(2\mu) - 1, \quad (12)$$

for Poisson's ratio (ν). Error propagation through Equations (11) and (12) was tested by adding 10% zero-mean random white noise to all the measured dynamic bulk and shear moduli in our dataset, resulting in less than 3% standard error for Young's modulus and 5% standard error for Poisson's ratio.

Combining Equations (9) and (10) with (11) and (12) allows computation of Young's modulus and Poisson's ratio as a function of fractional organic and clay volumes (Figures 8 and 9) as an indication of

relative changes. In these plots, we have restricted the maximum X_{TOC} to 0.2 so as not to extrapolate the results far from the average formation properties of the entire dataset.

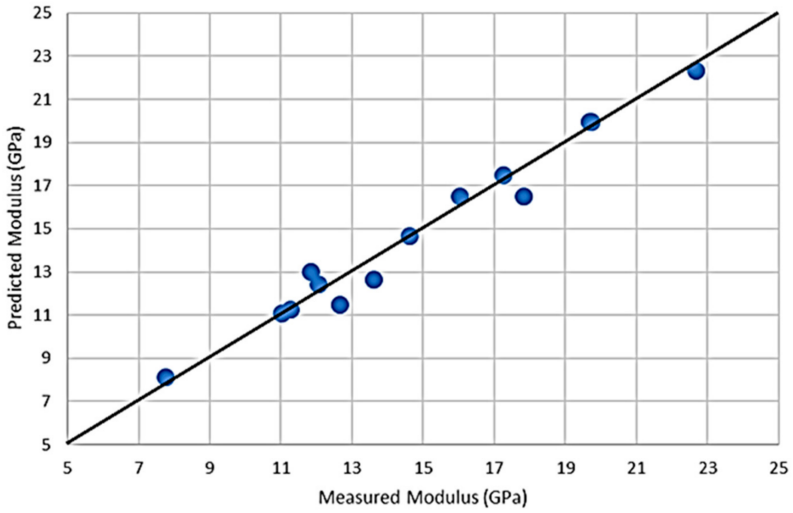

Figure 7. Measured versus predicted average formation dynamic bulk and shear moduli using Equations (9) and (10) and the data from Table 1. These equations indicate that average moduli are primarily dependent on volume fractions of clay and TOC. Despite ignoring other variables, they still match the observed average moduli with high correlation and a standard error within 1 GPa. All other variables surprisingly do not improve the fit or significance of the regressions. We suspect that geological correlations reduce the additional prediction error reduction that can be achieved by including factors such as porosity, fluid content, or effective pressure.

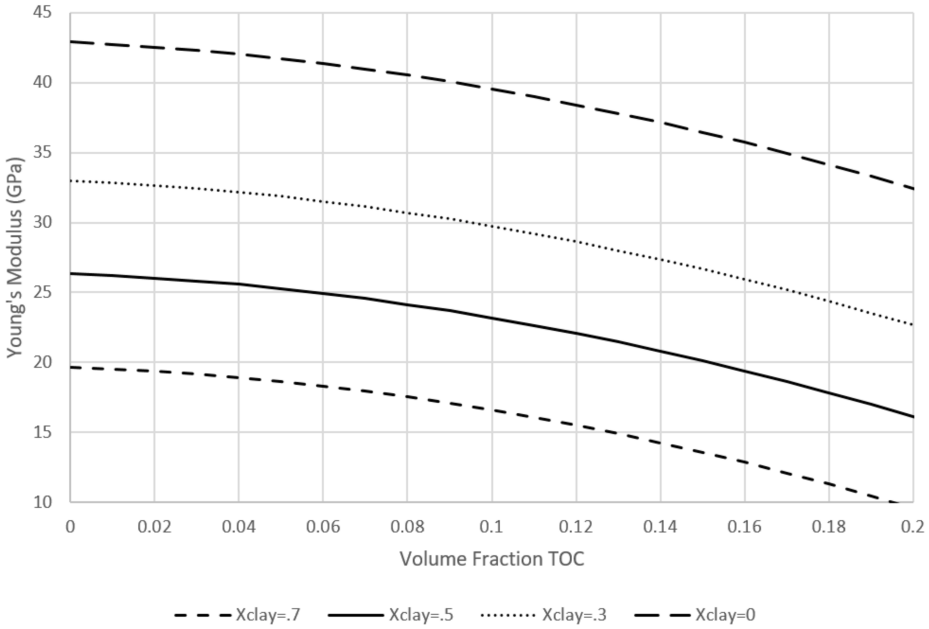

Figure 8. Relationship between Young's modulus and volume fraction of TOC for lines of constant clay content. Equations (9)–(11) are used to show the compositional dependence of Young's modulus. Lines are for different constant volume fractions of clay (X_{CLAY}) of 0.7 (dashed line), 0.5 (solid line), 0.3 (dotted line), and 0 (long dashed line) from the regression Equations (9) and (10) and elastic moduli relationships (11) and (12). These trends represent average shale reservoir properties in our dataset and may vary somewhat in different localities.

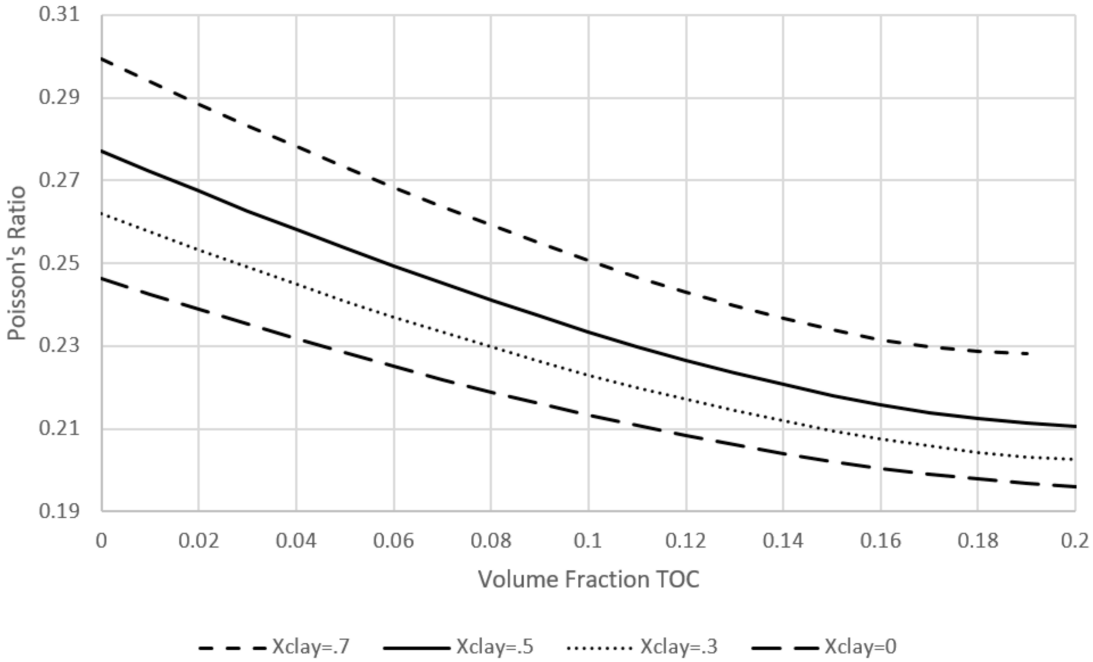

Figure 9. Relationship between Poisson's ratio and volume fraction of TOC for lines of constant clay content. Equations (9), (10) and (12) are used to show the compositional dependence of Poisson's ratio. Lines are for different constant volume fractions of clay (X_{CLAY}) of 0.7 (dashed line), 0.5 (solid line), 0.3 (dotted line), and 0 (long dashed line) from the regression Equations (9) and (10) and elastic moduli relationships (11) and (12). These trends represent average shale reservoir properties in our dataset and may vary somewhat in different localities.

In agreement with laboratory measurements [7], Young's modulus decreases monotonically with increasing volume fractions of clay or organic matter (Figure 8). At a given organic volume fraction, increasing the clay volume fraction from 0% to 50%, drops the Young's modulus almost in half. The absolute change in Young's modulus with organic matter volume is virtually independent of clay volume. As a result, for higher clay volumes the percent change in Young's modulus with organic matter is much greater than for low clay volumes. Poisson's ratio increases with clay volume fraction and decreases with TOC (Figure 9) although the percent change is much smaller for Poisson's ratio than for Young's modulus. The magnitude of the increase in Poisson's ratio with clay volume fraction is reduced at higher TOC where Poisson's ratio becomes relatively insensitive to changing TOC as the curves flatten out.

Using these same equations and varying clay volume fraction from 0 to 0.7, the cross-plot of Poisson's ratio versus Young's modulus for lines of constant TOC volume (Figure 10) shows that (1) the variation in Young's modulus is much greater than that for Poisson's ratio and (2) Young's modulus and Poisson's ratio both decrease with increasing TOC. For reservoir rocks with high Young's modulus and low clay content, the relationship between Young's modulus and Poisson's ratio at a given TOC is almost linear.

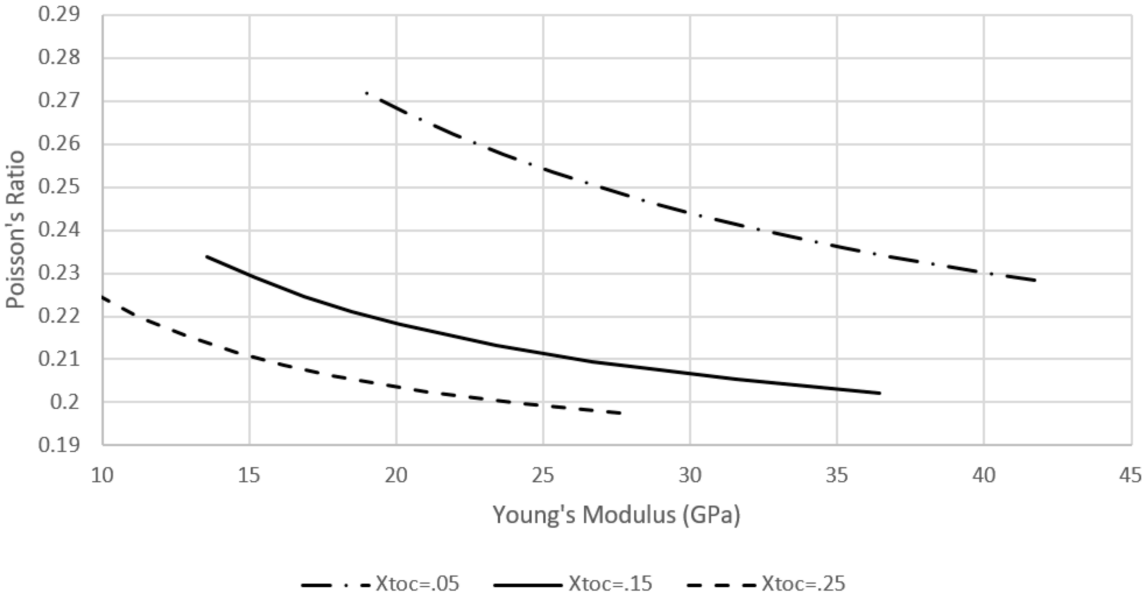

Figure 10. Relationships between Poisson's ratio and Young's modulus. Equations (9)–(12) are used to show the dependence of the relationship between these moduli on the volume fraction of TOC. Lines are for constant TOC volume fractions (X_{TOC}) of 0.25 (dashed line), 0.15 (solid line), and 0.05 (dot-dash line) from the regression Equations (9) and (10) and elastic moduli relationships (11) and (12). These trends represent average shale reservoir properties in our dataset and may vary somewhat in any given locality.

4. Discussion

The effect of fluids (or lack thereof) is conceptually easy to understand and, to first order at least, behaves in the way physical equations suggest in shale reservoirs [9]. Ignoring geological diagenesis and geochemical effects, the mechanics of Biot-Gassman theory [34,35] tells us that for a given rock frame compressibility, the more compressible the fluid, the more compressible the fluid saturated rock. Thus, all else being equal, a gas-saturated rock should have a lower k/μ ratio than a light oil-saturated rock with high gas–oil-ratio (GOR), which in turn should have a lower k/μ ratio than a black oil reservoir with low GOR. It is also generally accepted [36] that Gassmann's equations are applicable at sonic frequencies in permeable sandstones. Within the context of his assumptions, Gassmann [35] proves that shear modulus should be unaffected by the pore fluid compressibility. This may not be entirely true if non-spherical pores are acoustically disconnected and pressures cannot equilibrate, but we will accept this as a working hypothesis with the assumption that, if the hydrocarbons are indeed flowable, then there is pressure communication between pores and Gassmann's equations apply. It has also been shown [37] that if similar low-aspect ratio pores are aligned, as one might expect them to be for the most part in shales, that Gassmann's equations, which are the low frequency limit of the more general Biot theory, are applicable and shear modulus is mechanically independent of fluid compressibility. This is because the pores deform to the same degree for a given applied stress and pressure equilibration between pores is achieved without requiring actual fluid communication. In organic shales, [9] reported bulk modulus variation with fluid saturation from fully brine-saturated to hydrocarbon saturated, but no such dependency for shear modulus. The effect of pore fluids on a k versus μ cross-plot, should then be entirely on k while leaving μ unchanged. This would of course change the k versus μ relationship. However, regressions (9) and (10) for data entirely within hydrocarbon saturated reservoir rocks show no dependency of either bulk modulus or shear modulus with fluid properties and saturations. The change in bulk modulus from hydrocarbons saturated to fully brine-saturated, should be generally larger than the change in bulk modulus as hydrocarbon saturation varies within a reservoir. As we have excluded datapoints with brine-saturations greater

than 70% from regression analysis, the fluid effect on rock bulk modulus as saturation varies should be small. In addition, the effects of interrelated parameters such as pore fluid saturation and TOC are not readily separated by multiple linear regression in these data and may mask any small fluid modulus effect. Controlled laboratory experiments, though difficult to perform in shales, are needed to separate the direct effect of varying fluid modulus from that of solid organic matter volume fraction.

Equations (7) and (8), both using the dynamic P-wave modulus, are the most promising for prediction of the variation of bedding normal dynamic shear modulus throughout a reservoir with limited information, and for application without local calibration. To apply Equation (7), only compressional-wave sonic and density logs are required. Equation (8) requires these and volumetric well log analysis compositions. Starting with P-wave modulus to predict shear modulus yields more universal relations because factors such as porosity, pore fluid content, effective pressure, degree of lithification and cementation, thermal maturity, pore and grain shape distribution, and structural arrangement and distribution of constituents are all reflected to some degree in the P-wave modulus. Within reservoir rock they do not apparently change the relationships between P-wave modulus and shear modulus to the extent that compositional variables do. The most important compositional variables are fractional volumes of solid organic matter, clay, and carbonates. As fractional volumes sum to one, the fractional quartz volume is reflected in the other constituent volumes and can be thought of as the background giving the regression intercept which is modified by the other compositions.

Figure 11 compares observed versus predicted shear moduli using P-wave modulus alone (Equation (7)) and using modulus and composition (Equation (8)). A perfect prediction would have a regression trendline between observation and prediction along the diagonal with a slope of 1 and an intercept of 0. Using P-wave modulus alone (Figure 11a) gives a trendline slope of 0.85, an intercept of nearly 2 GPa, and a squared correlation coefficient (R^2) of 0.85; a good prediction with slope and intercept not far from unity and zero, but suggesting bias manifesting as an underestimation of large shear moduli and overestimation of small moduli. Adding compositional information with Equation (8) improves R^2 to 0.88 with slope of 0.95 and intercept of −0.16 indicating less bias.

The fact that a regression equation yields on average accurate predictions of shear modulus for all the calibration data across all included formations does not mean that the depth-by-depth prediction of shear modulus will be acceptable over a given logged interval. This becomes important in intervals where compositions deviate significantly from the average composition in the calibration dataset. For example, Figure 12 shows the observed dynamic shear modulus log in an interval of the Spraberry formation. The predicted shear modulus using only P-wave modulus is clearly overestimated in the intervals of lower shear modulus while the prediction incorporating compositional information is generally better.

We performed out-of-sample validation on measurements available in the literature to test the applicability of Equations (7) and (8) in different localities, different formations, and with different measurement methods (laboratory versus log). Unfortunately, tabulated moduli and compositions are not common, so in some cases we had to read values from logs or take averages to get representative values. Compositions on lab samples are also problematical because those reported are not necessarily for the same piece of rock the measurements are made on. Table 6 lists the samples we use for validation. Figure 13 shows that moduli predicted for these samples using Equations (7) and (8) have standard error of around 1.5 GPa, an acceptable result especially given the variety of unknowns associated with using measurements from other sources that may result in inconsistencies. For example, the laboratory measurements were made on dry samples rather than under in situ conditions, and log compositional analysis can be variable depending on how constituents are defined or lumped. In log analysis, it is not uncommon for there to be inconsistencies in the definition of clay volume or in how feldspars of various kinds are handled. Considering these uncertainties and the small sample size for this test we do not judge the difference in standard error between the methods to be significant. The good correlation (R^2 = 0.95) between predicted and observed moduli for both Equations (7) and (8) suggests that the use of P-wave modulus is robust without local calibration.

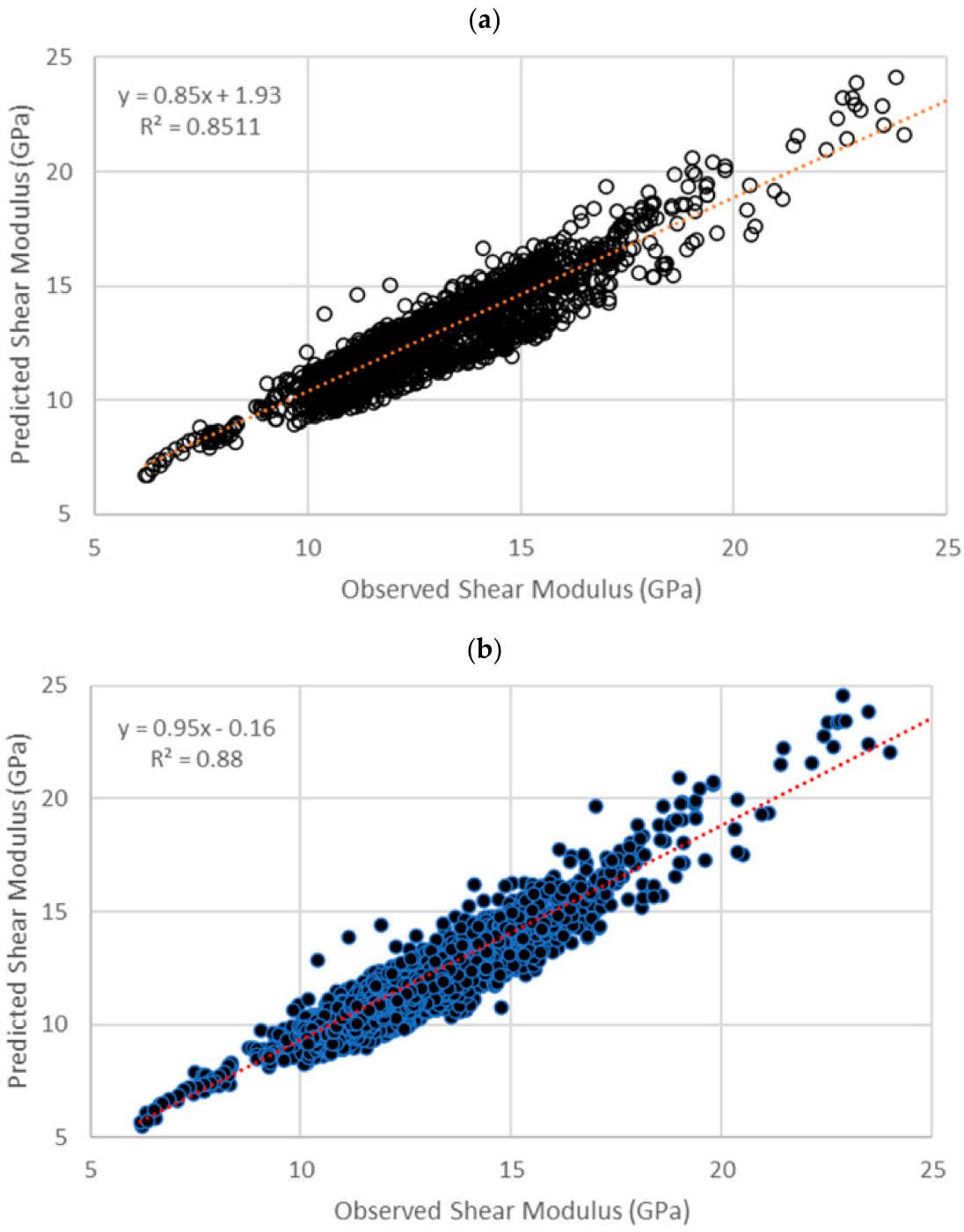

Figure 11. Predicted versus observed dynamic shear moduli. (**a**) using only P-wave modulus with Equation (7), and (**b**) using P-wave modulus, and fractional volumes of TOC, clay, and carbonate with Equation (8). The prediction using P-wave modulus and composition has a higher correlation, a smaller standard error, and is closer to the diagonal (exhibiting less bias for small and large moduli).

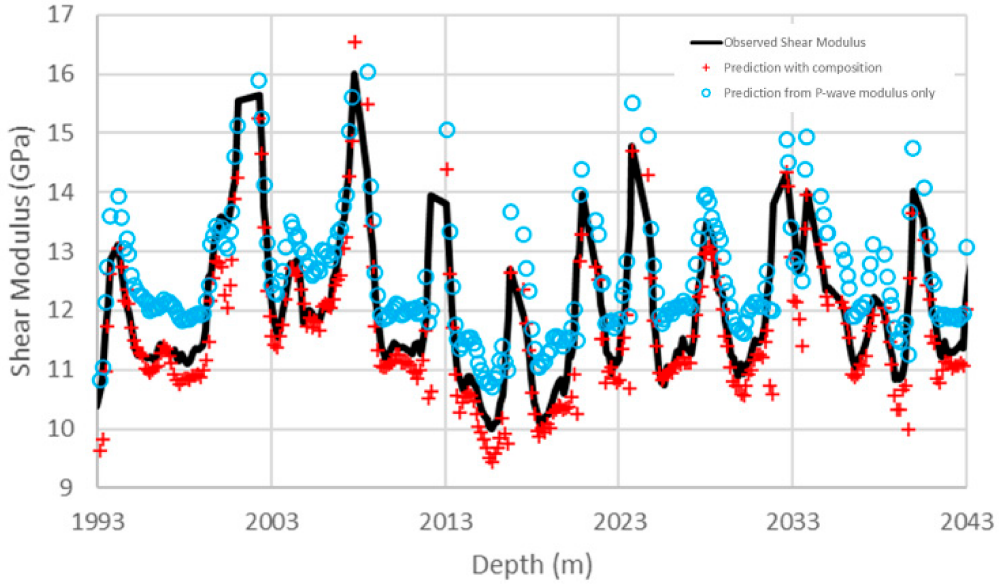

Figure 12. Observed and predicted dynamic shear moduli in an interval of the Spraberry formation. The observed shear modulus log (black line) is straight lined over intervals where logged data were excluded due to high water saturation or low TOC. Predictions are absent in those intervals. The prediction using P-wave modulus alone (open blue circles) with Equation (7) is biased towards higher shear moduli while the prediction with Equation (8) using P-wave modulus and composition (red plus signs) is on average significantly more accurate over this interval. It is significant that the compositional coefficients for Equation (8) were obtained for the entire dataset, including all seven formations, rather than locally calibrated.

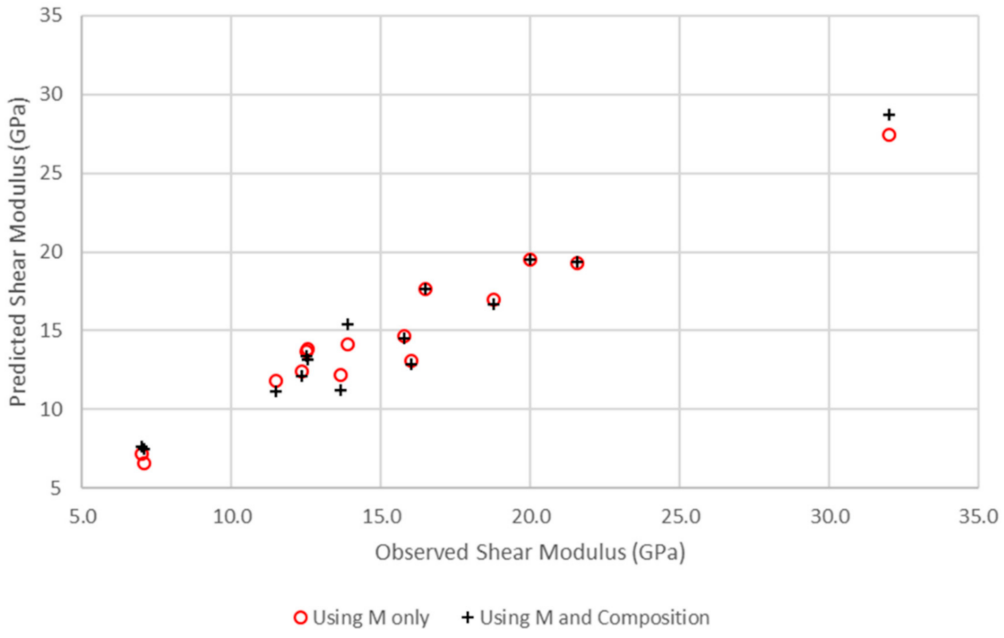

Figure 13. Comparison of predicted and observed dynamic shear moduli for the out-of-sample literature data provided in Table 6. The open red circles are for predicted shear moduli made only with P-wave modulus with Equation (7). The black plus signs are for predicted shear moduli using P-wave modulus and volume fractions of solid organic matter, clay, and carbonate with Equation (8). The predictions are excellent excepting the single datapoint with anomalously high shear modulus. The standard error is 1.5 GPa using Equation (8) and 1.6 GPa using Equation (7). R^2 is 0.95 for both predictions.

Table 6. Literature data used for validation. These data are from different formations than those included in our database, or from the same formation but from different localities, or acquired in the laboratory; each instance thereby constituting an out-of-sample test. Moduli are in GPa, density is in gm/cc, and volume fractions are normalized to sum to one.

Formation	Type	Reference	ρ	M	u	X_{TOC}	X_{Clay}	X_{Quartz}	X_{Carb}	u
Bakken	log	27	2.18	15.9	7.1	0.26	0.21	0.38	0.15	7.1
Marcellus 1	log	27	2.55	34.9	12.3	0.10	0.37	0.43	0.10	12.3
Marcellus 2	log	27	2.28	17.9	7.0	0.23	0.32	0.37	0.08	7.0
Spraberry	lab	9	2.57	57.4	21.6	0.02	0.28	0.67	0.03	21.6
Spraberry	lab	9	2.49	42.2	15.8	0.06	0.32	0.59	0.02	15.8
Spraberry	lab	9	2.55	49.7	18.8	0.02	0.32	0.62	0.04	18.8
Longmaxi	log	21	2.60	39.5	12.6	0.10	0.53	0.26	0.11	12.6
Longmaxi	log	21	2.41	40.5	13.9	0.19	0.19	0.57	0.05	13.9
Barnett 2	lab	6	2.65	84.0	32.0	0.03	0.05	0.43	0.49	32.0
Barnett 1	lab	6	2.43	37.0	16.0	0.10	0.38	0.51	0.02	16.0
Haynesville 1	lab	6	2.50	33.0	11.5	0.08	0.38	0.34	0.21	11.5
Haynesville 2	lab	6	2.61	58.0	20.0	0.04	0.21	0.24	0.51	20.0
Eagleford 1	lab	6	2.45	39.0	12.5	0.06	0.17	0.26	0.51	12.5
Eagelford 2	lab	6	2.50	52.0	16.5	0.05	0.10	0.15	0.71	16.5
Longmaxi	log	38	2.35	34.1	13.6	0.11	0.63	0.27	0.00	13.6

5. Conclusions

We performed linear regression of sonic log compressional and shear-wave bedding normal velocities in single vertical wells from each of seven different unconventional shale reservoirs: the Spraberry, Wolfcamp, Avalon, Woodford, Eagle Ford, Cline, and Bakken formations.

Overall, and in each of these formations, relationships between compressional and shear-wave velocities are well defined. Compressional-wave velocity is an excellent predictor of shear-wave velocity with a correlation coefficient of 0.9 and a mean absolute error of 2.9% when using a single equation for all seven reservoirs; when regressing individually for each reservoir the mean absolute error is 1.7%.

Combined with a bulk density log, these velocities can be used to compute dynamic elastic moduli logs including bulk, shear, and Young's moduli and Poisson's ratio.

Using measured dynamic P-wave modulus to predict shear modulus results in a high correlation coefficient (0.92) with a standard prediction error of 0.92 GPa. Adding compositional variables to the regression improves the correlation coefficient to 0.95 and reduces the standard error to 0.77 GPa. Both regressions have high statistical significance with virtually nil probability of the correlations being spurious.

Using bulk modulus alone as a predictor of shear modulus and a single linear regression equation for all formations resulted in only a modest correlation (0.78) and relatively large error between measurements and predictions of nearly 3 GPa. The error can be improved using formation specific equations or regressing against volumetric compositional variables; the two most important being fractional volume of organic matter and volume of clay in that order.

While average formation bulk modulus was found to be linearly related to volume faction of TOC, average formation shear modulus is better predicted using the square of the volume fraction of TOC. Using a single regression equation and only compositional variables for all formations, standard prediction error was 1 GPa for average formation shear modulus and 0.75 GPa for bulk modulus. The regressions indicate that both Young's modulus and Poisson's ratio decrease with increasing TOC while increasing clay volume decreases Young's modulus and increases Poisson's ratio. Including other variables in the modulus regressions such as porosity, carbonate content, and fluid properties, and saturations did not improve the predictions appreciably and resulted in reduced statistical measures of significance. However, it is unlikely that regressions containing only compositional variables alone will remain valid outside of the calibration dataset due to variations in factors such as porosity, effective

stress, fluid content, degree of lithification, and hydrocarbon maturity. Predictions using the plane-wave modulus, with or without compositional information, promise to be more universally applicable.

Supplementary Materials: The following are available online at http://www.mdpi.com/1996-1073/13/22/6001/s1, Table S1: Regression data.

Author Contributions: Conceptualization, S.J.O. and J.P.C.; Data curation, S.J.O.; Formal analysis, S.J.O. and J.P.C.; Investigation, S.J.O.; Methodology, J.P.C.; Software, S.J.O.; Supervision, J.P.C.; Validation, S.J.O.; Visualization, S.J.O.; Writing—original draft, J.P.C. All authors have read and agreed to the published version of the manuscript.

Funding: This research received no cxternal funduing.

Conflicts of Interest: The authors declare no conflict of interest.

Appendix A Regression Statistics

The mean absolute error measures the average discrepancy magnitude between predicted and observed values. At a given depth, discrepancy may be due to inadequacies in the model, but also experimental error in the velocity measurements and the volumetric inputs to the velocity prediction. When mean error is near zero, the mean absolute error is thus a good indication of the precision of the method

$$\textit{Mean absolute error } = \frac{1}{N}\sum_{i=1}^{N}\left|p_i - m_i\right|, \tag{A1}$$

where N is the number of datapoints tested (observations), the p_i are the predicted moduli for each sample i and the m_i are the measured values for each sample.

The standard error is the square root of the variance of the prediction error and similarly an indication of precision when mean error is near zero.

$$\textit{Standard error} = \frac{1}{\sqrt{N-1}}\sqrt{\left(\sum_{i=1}^{N}\left(p_i - m_i\right)^2\right)} \tag{A2}$$

Fisher's F test statistic (F) is used to compare prediction models for fitting data as an indication of the significance of a correlation. For prediction models that fit calibration data equally well (same correlation coefficient and prediction error) the model with the greater F value is more statistically significant. In our application, we use F to determine if the regression model provides a better fit of the data than simply using the data mean. F is given by

$$F = (\mathrm{R}^2/K)/[(1-\mathrm{R}^2)/(N-K-1)] = \text{explained variance/unexplained variance}, \tag{A3}$$

where R is the correlation coefficient and K is the number of variables used to fit the data. In general, the more variables are required to achieve a given correlation and prediction error, or the fewer data points to be fit, the lower F. In the extreme case where the number of variables is one less than the number of data points to be fit, a perfect fit can be accomplished, but the denominator of (A3) goes to infinity and F is zero. For a given fit to the data, the higher F, the better the regression model. The 'art' of linear regression is then, for a given N, to achieve a balance between the correlation achieved and the number of variables used to achieve that correlation to maximize F. 'Overfitting' occurs when too many variables are used to fit a small number of datapoints yielding a small F. This often results in poor predictions for out-of-sample data not used in the calibration.

A spurious correlation is a high correlation achieved only by random chance. The fewer the datapoints to be fit, and the more variables available to fit those data, the greater the probability of a spurious correlation. The probability that the correlation achieved by a regression model is spurious is called the significance of F (sig F). In our application, sig F is the probability that the real coefficients of the independent variables are all zero, in which case no independent variables are useful and the mean of the data is a better estimator. Usually a sig F less than 0.05 is taken to mean that the hypothesis that

the regression coefficients are all zero and the regression is therefore not statistically significant can be rejected.

In this study, all regressions performed on moduli and volumetric logs were highly statistically significant with high *F* and low sig F. The significance was helped by the large number of datapoints relative to the number of variables in these cases. Numerous regression combinations, for example those involving porosity and fluid parameters, were rejected as having inferior statistical significance and were not presented here. On the other hand, regressions performed on average formation properties involved only seven data samples, and the number of regression variables had to be kept to a minimum to achieve acceptable significance tests (Table A1). Inspection of Table A1 suggests that Equation (7) using P-wave modulus alone as a variable is by far the most robust regression model while Equation (8), which adds compositional variables, matches the data best, and retains very high statistical significance.

Table A1. Summary of modulus regression statistics. *N* is the number of observations. *K* is the number of variables in the model. Units of standard error (Std Error) are GPa. Ris the correlation coefficient between observations and predictions. Std Error is given by Equation (A2). *F* is the Fisher coefficient and sig *F* is the significance of the regression.

Regression Model	N	K	R	Std Error	F	Sig F
Equation (6)	2038	1	0.78	2.79	3000	0.000
Equation (7)	2038	1	0.92	0.92	11,000	0.000
Equation (8)	2038	4	0.95	0.77	4424	0.000
Equation (9)	7	2	0.99	0.75	69	0.001
Equation (10)	7	2	0.93	1.0	12	0.020

References

1. King, M.S. Static and dynamic elastic moduli of rocks under pressure. In Proceedings of the 11th U.S. Symposium on Rock Mechanics (USRMS), Berkeley, CA, USA, 16–19 June 1969; ARMA-69-0329.
2. Belyadi, H.; Fathi, E.; Belyadi, F. *Hydraulic Fracturing in Unconventional Reservoirs, Theories, Operations, and Economic Analysis*, 2nd ed.; Elsevier: Amsterdam, The Netherlands, 2019; p. 614.
3. Gregory, A.R. Aspects of rock physics from laboratory and log data that are important to seismic interpretation. *Seism. Stratigr. Appl. Hydrocarb. Explor.* **1977**, *26*. [CrossRef]
4. Tixier, M.; Loveless, G.; Anderson, R. Estimation of formation strength from the mechanical-properties log (incudes associated paper 6400). *J. Pet. Technol.* **1975**, *27*, 283–293. [CrossRef]
5. Rickman, R.; Mullen, M.; Petre, E.; Grieser, B.; Kundert, D. Practical use of shale petrophysics for stimulation design optimization—All shale plays are not clones of the Barnett Shale. In Proceedings of the SPE Annual Technical Conference and Exhibition, Denver, CO, USA, 21–24 September 2008.
6. Sone, H.; Zoback, M.D. Mechanical properties of shale-gas reservoir rocks—Part 1: Static and dynamic elastic properties and anisotropy. *Geophysics* **2013**, *78*, D381–D392. [CrossRef]
7. Ong, O.N.; Schmitt, D.R.; Kofman, R.S.; Haug, K. Static and dynamic pressure sensitivity anisotropy of a calcareous shale. *Geophys. Prospect.* **2016**, *64*, 875–897. [CrossRef]
8. Greenberg, M.L.; Castagna, J.P. Shear-wave velocity estimation in porous rocks: Theoretical formulation, preliminary verification and applications. *Geophys. Prospect.* **1992**, *40*, 195–209. [CrossRef]
9. Omovie, S.J.; Castagna, J. P-to-S-wave velocity ratio in organic shales. *Geophysics* **2019**, *84*, MR205–MR222. [CrossRef]
10. Harris, N.B.; Moghadam, A.; Dong, T. The effects of organic carbon content and thermal maturity on acoustic parameters in a black shale: Woodford Shale, Permian Basin, West Texas. *Geophysics* **2019**, *84*, D231–D248. [CrossRef]

11. Lucier, A.M.; Hofmann, R.; Bryndzia, L.T. Evaluation of variable gas saturation on acoustic log data from the Haynesville Shale gas play, NW Louisiana, USA. *Leading Edge* **2011**, *30*, 300–311. [CrossRef]
12. Vernik, L.; Milovac, J. Rock physics of organic shales. *Leading Edge* **2011**, *30*, 318–323. [CrossRef]
13. Alfred, D.; Vernik, L. A new petrophysical model for organic shales. In Proceedings of the 53rd Annual Logging Symposium Transactions, Cartagena, Columbia, 16–20 June 2012; pp. 2012–2217.
14. Sayers, C.M. The effect of kerogen on the elastic anisotropy of organic rich shales. *Geophysics* **2013**, *78*, D65–D78. [CrossRef]
15. Hu, R.; Vernik, L.; Nayvelt, L.; Dicman, A. Seismic inversion for organic richness and fracture gradient in unconventional reservoirs: Eagle Ford Shale, Texas. *Leading Egde* **2015**, *34*, 80–84. [CrossRef]
16. Altowairqi, Y.; Rezaee, R.; Evans, B.; Urosevic, M. Shale elastic property relationships as a function of total organic carbon content using synthetic samples. *J. Pet. Sci. Eng.* **2015**, *133*, 392–400. [CrossRef]
17. Jiang, M.; Spikes, K.T. Rock-physics and seismic-inversion based reservoir characterization of the Haynesville Shale. *J. Geophys. Eng.* **2016**, *13*, 220–233. [CrossRef]
18. Szewczyk, D.S.; Bauer, A.; Holt, R.M. Stress-dependent elastic properties of shales—Laboratory experiments at seismic and ultrasonic frequencies. *Geophys. J. Int.* **2017**, *212*, 189–210. [CrossRef]
19. Gong, F.; Di, B.; Wei, J.; Ding, P.; Pan, X.; Zu, S. Ultrasonic velocity and mechanical anisotropy of synthetic shale with different types of clay minerals. *Geophysics* **2018**, *83*, MR57–MR66. [CrossRef]
20. Hansen, J.A.; Mondol, N.H.; Fawad, M. Organic content and maturation effects on elastic properties of source rock shales in the Central North Sea. *Interpretation* **2019**, *7*, T477–T497. [CrossRef]
21. Deng, X.; Liu, C.; Guo, Z.; Liu, X.; Liu, Y. Rock physical inversion and quantitative seismic interpretation for the Longmaxi shale gas reservoir. *J. Geophys. Eng.* **2019**, *16*, 652–665. [CrossRef]
22. Xie, J.; Cao, J.; Schmitt, D.R.; Di, B.; Xiao, L.; Wang, X.; Wang, K.; Chen, Y. Effects of Kerogen Content on Elastic Properties-Based on Artificial Organic-Rich Shale (AORS). *J. Geophys. Res. Solid Earth* **2019**, *124*, 12660–12678. [CrossRef]
23. Iwuoha, S.; Pedersen, P.K.; Clarkson, C.R.; Gates, I.D. A working method for estimating dynamic shear velocity in the montney formation. *MethodsX* **2019**, *6*, 1876–1893. [CrossRef]
24. Sohail, G.M.; Hawkes, C.D. An evaluation of empirical and rock physics models to estimate shear wave velocity in a potential shale gas reservoir using wireline logs. *J. Pet. Sci. Eng.* **2020**, *185*, 106666. [CrossRef]
25. Venieri, M.; Weir, R.; Mckean, S.H.; Pedersen, P.K.; Eaton, D.W.S. Determining elastic properties of organic-rich shales from core, wireline logs and 3-D seismic: A comparative study from the Duvernay play, Alberta, Canada. *J. Nat. Gas Sci. Eng.* **2020**, *84*, 103637. [CrossRef]
26. Castagna, J.P.; Batzle, M.L.; Eastwood, R.L. Relationships between compressional-wave and shear-wave velocities in clastic silicate rocks. *Geophysics* **1985**, *50*, 571–581. [CrossRef]
27. Vernik, L.; Castagna, J.; Omovie, S.J. S-wave velocity prediction in unconventional shale reservoirs. *Geophysics* **2017**, *83*, MR35–MR45. [CrossRef]
28. Hmadov, J.; Mokhtari, M. Experimental evaluation of ultrasonic velocities and anisotropy in the Tuscaloosa marine shale formation. *Interpretation* **2020**, *8*, 1–62. [CrossRef]
29. Sondergeld, C.H.; Rai, C.S. Elastic anisotropy of shales. *Geophysics.* **2011**, *30*, 324–331. [CrossRef]
30. Vernik, L. *Seismic Petrophysics in Quantitative Interpretation*, 2nd ed.; SEG: Tulsa, OK, USA, 2016.
31. Batzle, M.; Wang, Z. Seismic properties of pore fluids. *Geophysics* **1992**, *57*, 1396–1408. [CrossRef]
32. Gardner, G.H.F.; Gardner, L.W.; Gregory, A.R. Formation velocity and density—The diagnostic basics for stratigraphic traps. *Geophysics* **1974**, *39*, 770–780. [CrossRef]
33. Eshkalak, M.O.; Mohaghegh, S.D.; Esmaili, S. Geomechanical Properties of Unconventional Shale Reservoirs. *J. Pet. Eng.* **2014**, *2014*, 1–10. [CrossRef]
34. Biot, M. Theory of propagation of elastic waves in a fluid-saturated porous solid I. Low-frequency range. *J. Acoust. Soc. Am.* **1956**, *28*, 168–178. [CrossRef]
35. Gassmann, F. Uber die elastizitat poroser medien. *Vierteljahrschrift der Naturforschenden Gessellschaft in Zurich* **1951**, *96*, 1–12.

36. Geertsma, J.; Smit, D.C. Some aspects of elastic wave propagation in fluid–saturated porous solids. *Geophysics* **1961**, *26*, 169–181. [CrossRef]
37. Grechka, V. Fluid-solid substitution in rocks with disconnected and partially connected porosity. *Geophysics* **2009**, *74*, WB89–WB95. [CrossRef]